Proceedings of 2003 Tyrrhenian International Workshop on Remote Sensing, E. Dalle Mese (Ed.), pp. 134-143, Edizioni Plus, University of Pisa, Italy, 2003. ISBN 88-8492-291-7

MULTIPLE SATELLITE OBSERVATIONS OF OCEANIC PLANETARY WAVES: TECHNIQUES AND FINDINGS

Paolo Cipollini

Southampton Oceanography Centre, cipo@soc.soton.ac.uk

Abstract

Recent satellite-based observations of oceanic planetary waves have improved our knowledge of the wave properties and lead to advancements in the theory. Firstly, we review some of the techniques adopted to extract the information on planetary wave properties, illustrating them with examples based on satellite altimeter data, and we summarize the main findings. Then we discuss a cross-spectral approach for the comparison of the wave signals in the different datasets (altimetry, ocean colour and sea surface temperature) that is necessary to unveil the causes of the newly found wave signature in satellite-derived maps of phytoplankton chlorophyll, a discovery that is attracting considerable interest as it implies some effects of the waves on biology.

Introduction and purpose of the work

In recent years, satellites have allowed an unprecedented study of planetary waves (also known as Rossby waves) in the oceans. These waves are a key dynamical phenomenon owing their existence to the conservation of potential vorticity (akin to angular momentum) and in turn to the rotation and shape of our planet, and have significant effects on the large scale ocean circulation and on the transport of climatic information across the main ocean basins (see for instance Gill, 1982). Planetary waves are essentially internal waves, that is disturbances in the vertical density field, also present in the atmosphere. In the oceans, they travel from east to west at speeds of the order of a few cm/s (depending on latitude: they go faster closer to the equator) and can take months or years to cross the main oceanic basins. The considerable difference in the horizontal and vertical scales of the waves is what makes them so hard to pin down with *in situ* observations: while the typical horizontal scale (corresponding to wavelength if the phenomenon were periodic) is hundreds or thousands of km, the vertical amplitude of the oscillation is a few tens of meters at the depth of the thermocline and the signature of the wave in the sea surface elevation is only a few centimetres. Thus it is not surprising that planetary waves, easily observed in the atmosphere since their discovery by Carl-Gustav Rossby in the 1930s, have eluded observation in the oceans until recently.

This dearth of observations came to an end with the arrival of satellite altimetry in the 1990s, when the availability of accurate sea surface height observations from

TOPEX/Poseidon (T/P) and ERS-1 and -2 allowed a convincing demonstration of the ubiquity of planetary waves at mid-latitudes in the oceans (Chelton and Schlax, 1996), and the study of their propagation characteristics. It was found that waves propagate up to 2-3 times faster than was previously thought from the existing theory, a fact that has important implications for the response time of the oceans to forcing. This noticeable discrepancy has driven scientists to improve the theoretical framework (Killworth et al., 1997, Killworth and Blundell, 2003a, 2003b) resulting in a better match between the predicted and observed speeds.

Another remarkable observational result was the identification of different wave modes in the satellite data. Theory suggests that the wave signal is the superposition of several propagating modes, each one having a different vertical structure. The vertically uniform (or *barotropic*) mode propagates fast (hundreds or thousands of cm/s) and it is difficult to view in satellite data lacking sufficient temporal resolution. Of the vertically variable (known as *baroclinic*) modes, the first one is normally the most important. The speeds of the baroclinic modes are of the order of a few cm/s and decrease with mode number. Case studies using both altimeter and Sea Surface Temperature (SST) data showed evidence of the first three modes in some locations (Cipollini et al., 1997; Subrahmanyam et al., 2001).

Accurate inspection of global data from satellite instruments other than altimeters has shown that the signature of planetary waves is ubiquitous in those datasets too. Hill et al. (2000) proved that the waves are visible almost everywhere in the SST record, using infrared data collected by the Along-Track Scanning Radiometer (ATSR) on board the ERS satellites. Cipollini et al. (2001) and Uz et al. (2001) showed that the waves are also visible in ocean colour data, which opens captivating questions (Siegel, 2001) about the mechanisms by which the waves affect phytoplankton, questions tackled by a most recent paper by Killworth et al. (2003).

As the information about the waves in the various satellite datasets is blended together with the signals deriving from other large-scale and meso-scale phenomena, the successful identification of the waves and quantification of their characteristics requires a number of specialized signal processing techniques, capable of extracting the information on the propagating disturbances. Some procedures are also needed for the comparison of the wave signature in the different datasets. In this work we aim at reviewing the techniques commonly adopted for the study of planetary waves, some of which have been developed specifically for this task. We will also summarize the main findings on planetary waves that have been obtained by applying those techniques.

Observations from altimetry and techniques for wave detection and analysis

Due to their east to west propagation, planetary waves are easily observed in longitude-time sections of Sea Surface Height Anomaly (SSHA) data from polar-

orbiting altimeters. Figure 1a, a longitude-time diagram of SSHA at 25°S across the Atlantic Ocean, shows clear westward propagating signals, corresponding to the surface signature of the planetary waves, as diagonal alignments of positive and negative anomalies across the plot. The slope of the alignments indicates their speed, which is around 6-7 cm/s in this example. The waves can be highlighted with appropriate 2-D band-pass filtering on the plot, as shown in figure 1b where only wavelengths between 3° and 15° in longitude and periods between 120 and 540 days have been preserved.

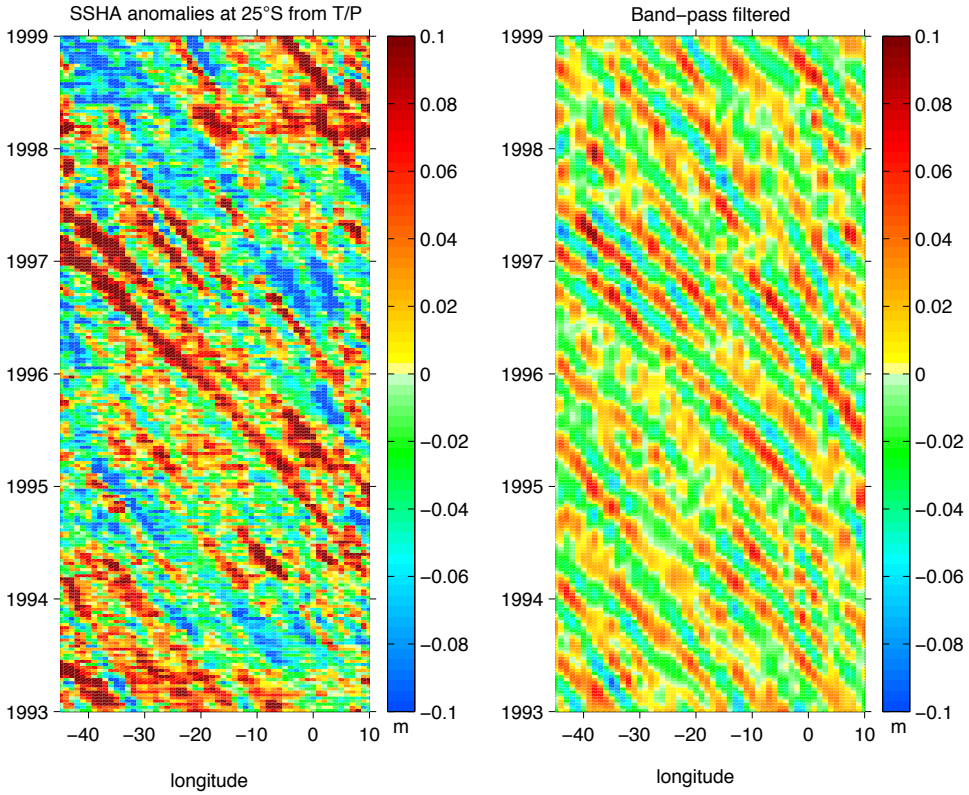

Figure 1. a) Longitude-time diagram of SSHA at 25°S across the Atlantic Ocean; b) same as in a), after band-pass filtering at wavelengths between 3° and 15° degrees longitude and periods between 120 and 540 days.

It should be noted that the propagating positive or negative disturbances do not necessarily repeat themselves with strict periodicity; in some cases single wave events can be observed in the data. In those locations where the waves can be considered periodic or quasi-periodic, a natural way of obtaining information on the frequency and wavenumber of the propagating components (thus allowing the identification of the single propagating modes) is 2-D spectral analysis of the lon-

gitude-time diagrams. Figure 2 shows the Power Spectral Density (squared modulus of the 2-D Fourier Transform) of the plot in figure 1b and highlights the different propagation components that may correspond to different propagation modes. An alternative approach, capable of yielding more localized information on the wave characteristics, is the wavelet transform (see for instance an application example in Cromwell, 2001).

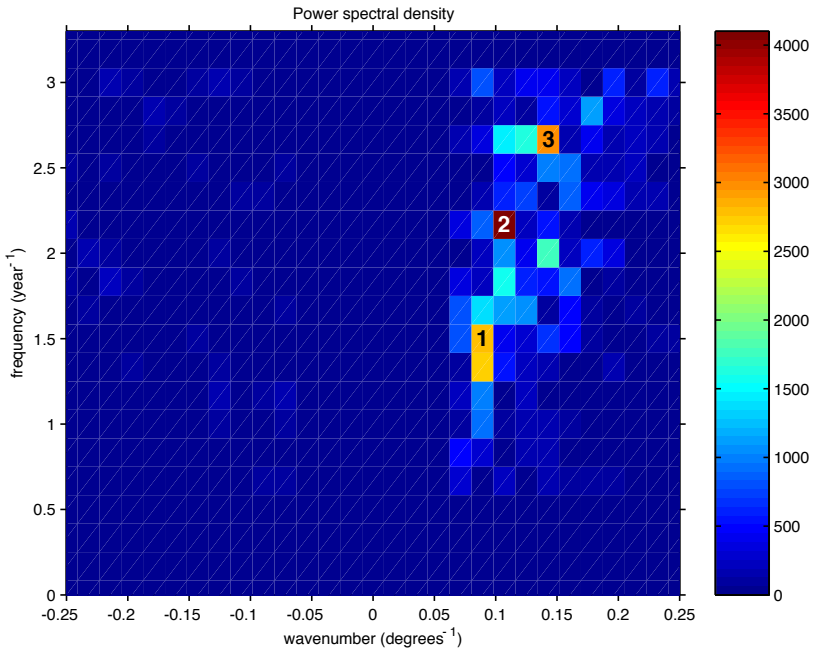

Figure 2. Portion of the Power Spectral Density (squared modulus of the 2-D Fourier Transform) of the plot in figure 1b, showing the main westward-propagating peaks. The three main peaks are 1) 11° and ~240 days, 2) 9.3° and ~170 days 3) 7° and ~140 days.

As discussed above, the wave speed is a parameter of key interest to oceanographers; as a consequence, objective methods are needed for its accurate estimation. One such method is the Radon Transform (RT) of the longitude/time diagrams, a technique widely used in geophysical data processing for its ability to find alignments in the data. The RT of an image at an angle θ (denoted with $P(x',\theta)$, see schematic in figure 3), is the projected integral of the image on a line oriented at angle θ with respect to the x axis; x' is the hybrid coordinate on the projection line (for more details on the RT see Deans, 1983). As indicated by the *projection-slice theorem*, the RT of an image at angle θ corresponds to the inverse Fourier transform of a section at the same angle θ in Fourier space. Hence, in practice, comput-

ing the Radon transform for different values of θ corresponds to scanning the Fourier space along sections through the origin and oriented at θ with respect to the wavenumber axis. The energy of the RT is maximum when the projection line is orthogonal to the predominant direction of the alignments on the plot and thus that particular θ can be readily converted into an objective estimate for the main propagation speed.

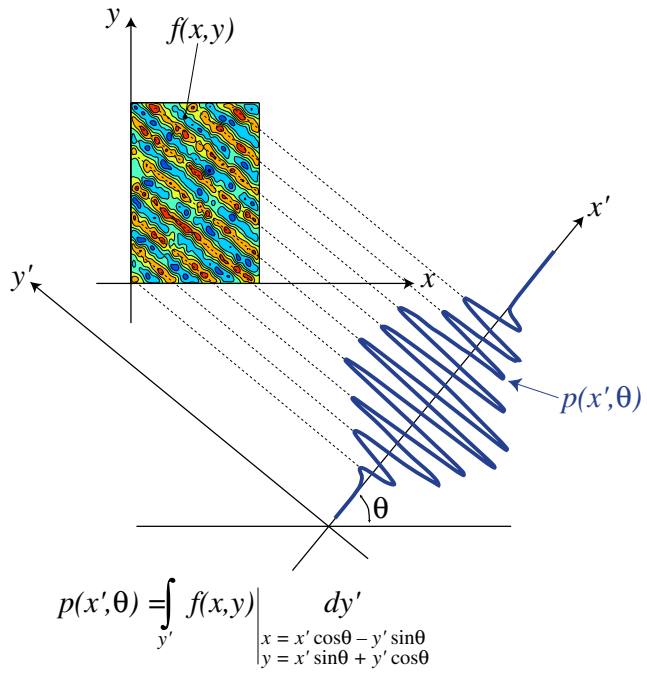

Figure 3. Schematic of the 2-D Radon Transform. (From Challenor et al., 2001)

Some studies carried out recently have aimed at removing the assumption of pure east-west propagation of the waves, and at analyzing full 3-D (longitude × latitude × time) cuboids of data in order to investigate the importance of any north-south component in the wave propagation. Apart from the immediate application of 3-D Fourier techniques to the cuboid, an effective way to tackle the problem is the extension of the RT to 3-D (Challenor et al., 2001) which is currently being applied to global altimetric datasets. This infers not only the speed of the waves, but also the true (i.e. not seen through a longitudinal section) direction of propagation of the disturbances. On this point, the new amendments to the theory (Killworth and Blundell, 1999, 2003a, 2003b) indicate that local deviations from a pure westward propagation may be induced by a number of causes including the bathymetry, but that the overall effect should be small. The first results by Challenor et al. (2001)

over the North Atlantic confirm the theoretical findings. In the 20°-40° latitude band, where most of the wave energy is concentrated, the main signals only show small localized deviations, but no coherent large-scale departure from pure westward propagation.

A more accurate characterization of the wave properties (especially for prognostic purposes, such as forecasting the propagation of planetary waves to predict their effect on density profiles or on the western boundary currents) requires the removal of the periodicity assumption and the identification and study of any individual wave event. A technique developed within the EU SOFT (Satellite-based Ocean ForecasTing) project consists of fitting a wave-shape model to the longitude-time plots of SSHA. The approach can be summarized as follows:

- split the full longitude/time plot at a given latitude into a number of overlapping sub-windows, which can be thought of as sub-setting the dataset by means of a window of width Λ degrees and moving by $\Delta\Lambda$ degrees at each step;
- for each sub-window, fit a number of elementary waves by minimizing the mean square error with respect to the wave shape model;
- reconstruct the trajectories of any single wave event by 'joining' the elementary waves in a sub-window with those in the adjacent window to the west;

A 2-D gaussian shape was chosen as it is easily tractable, and because preliminary tests showed that it fits the observed features well. Such a 2-D gaussian G is described by only 4 parameters, that is amplitude A, slope s, x-intercept p and width σ:

$$G = A\exp\left(-\frac{\left(x - t/s - p\right)^2}{2\sigma^2}\right)$$

where x is longitude and t time. Parameters s and p represent the slope and x-intercept of the line $t=s(x-p)$ representing the track of the propagating feature on the longitude-time plot; the slope s is thus linked to the speed of the feature. Parameter σ is a measure of the horizontal (east-west) scale of the feature. Tapered subsets of data (with a 11-point hanning window) are used in order to increase the localization of the estimation, and in the fitting code similarly tapered gaussians are fitted to the data. Tapering does improve the estimation of the local amplitude of the features (i.e. the amplitude near the longitudinal centre of the sub-window, which may differ from the 'mean' amplitude of a non-tapered feature).

The actual fitting is done with a Levenberg-Marquardt mean square error minimization algorithm, which obviously needs a quadruplet of parameters (A_0, s_0, p_0, σ_0) as a starting point. In the fitting scheme $|A_0|$ is set to 10 cm, σ_0 to 1° and the other two parameters are estimated by looking at the RT of the tapered sub-

window. The tapered gaussian whose initial slope and intercept correspond to the strongest peak in the RT is fitted first; then that elementary wave is removed from the tapered sub-window, and the fitting is iterated over the residual. When for a particular set of initial conditions the fitting algorithm either does not converge, or converges on a gaussian whose amplitude is below a threshold, the search is moved to the next largest peak in abs(RT). The amplitude threshold was taken as the largest between 2.5 cm and 0.8 times the standard deviation of the residual. This ensures that the largest amplitude features are fitted first. The iterative search exits (and moves to the next sub-window) when an acceptable solution cannot be found in the 5 largest peaks of abs(RT).

The reconstruction of the trajectories of any single wave event by 'joining' the elementary waves is carried out by starting from the easternmost sub-window and its associated table of elementary waves, each one identified by a (A, s, p, σ) set. Each one of these easternmost waves is labelled as 'new' and then compared with each elementary wave in the next window to the west by evaluating a cost function of the wave pair, depending on how well their amplitudes, slopes, positions (depending on slope and intercept) and widths match each other. In the cost function matrix F_c so obtained (where any row corresponds to an elementary wave in the new sub-window and any column to an elementary wave in the previous sub-window) the minimum cost is found, and if it is below an acceptance threshold the two waves are joined - that is, the elementary wave in the new sub-window is classified as a continuation of the one to the east, and the relevant row and column in the matrix are written off so that the two waves cannot be joined to any others. Once all the minima below the cost threshold in F_c have been accounted for, all the remaining waves are labelled as 'new' and the routine moves to the next sub-window to the west, and so on. The result is a structured table where any entry represents a 'joined' wave (that is, a single wave event made by one or more elementary waves), and lists the evolution of its parameters with longitude.

A visual example of some results from the application of the wave fitting routine to SSHA data at 34°N in the Atlantic is in figure 4. Figure 4a shows the original longitude-time plot. Figure 4b shows the crests and troughs identified by the technique (in red and blue, respectively) superimposed on the band-pass filtered longitude/time plot that has been input to the fitting routine. The thickness of any single wave line is proportional to the maximum amplitude reached by that wave. The evolution of a single wave event highlighted in figure 4b is presented in figure 5 and illustrates the potential of the technique in characterizing each specific wave. The results can be used to build a parameter space with all the values of the 4 parameters (A, s, p, σ) for any wave at a given longitude and the evolution of any new event can then be forecast by looking at the 'most similar' event(s) in the past, by defining an appropriate distance in the parameter space.

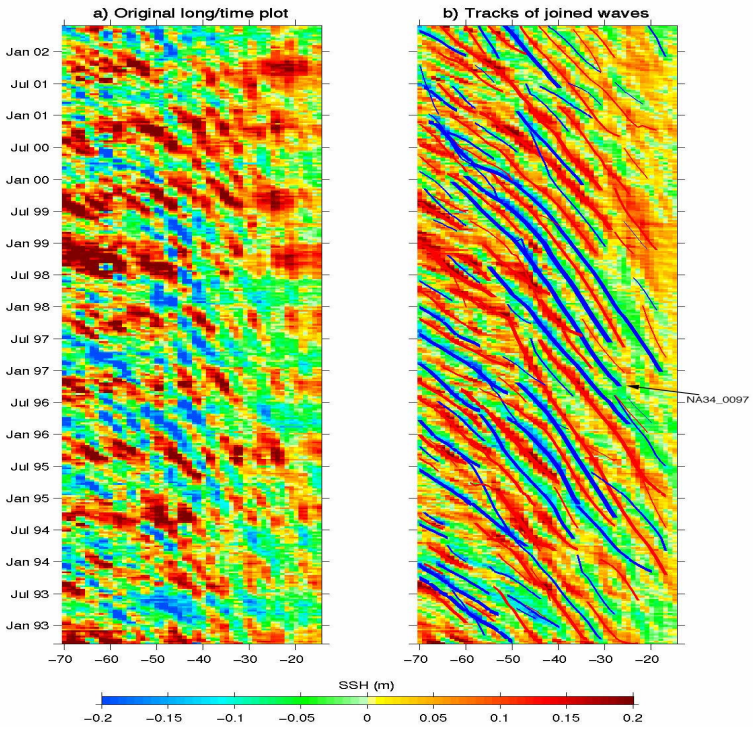

Figure 4. Example of application of the wave fitting routine to SSHA data from T/P. a) longitude/time plot at 34°N; b) tracks of those joined waves (red: crests; blue: troughs) propagating for at least 5° in longitude, superimposed on the band-pass filtered plot. The line width is proportional to the maximum amplitude of each wave.

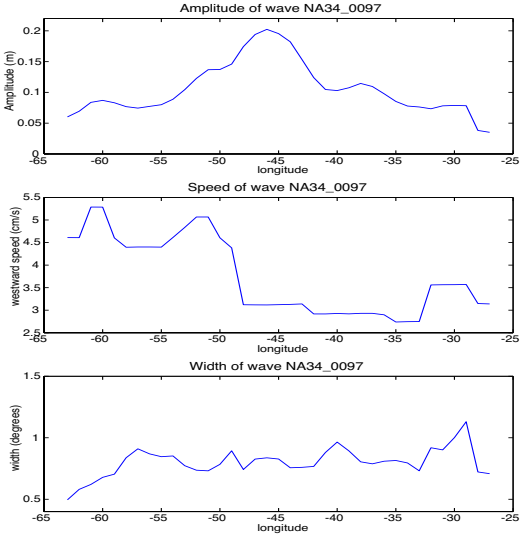

Figure 5. Parameters of wave NA34_0097 (see fig. 4b), as estimated by the fitting routine

Observations in SST and ocean colour and cross-spectral techniques

In addition to the global observations of planetary waves in SST by Hill et al. (2000), and in chlorophyll concentration from ocean colour sensors by Cipollini et al (2001) and Uz et al. (2001), other studies have investigated the occurrence of planetary waves at specific locations in concurrent SSHA, SST and ocean colour datasets. One illustrative example is the paper by Quartly et al. (2003), who analyse the signature of the waves at 34°S in the Indian Ocean and discuss some of the possible mechanisms for the presence of the signal in SST and ocean colour on the basis of the phase relationship and correlation between the different datasets.

The presence of a chlorophyll signal related to planetary waves is particularly intriguing, as it implies some effects of the waves on the biology, and may indicate potential repercussions on the carbon cycle. A new study by Killworth et al. (2003) sets out to investigate the possible causes for such a signature by means of joint satellite-derived SSHA/chl observations plus theoretical modelling. One of the techniques that can be adopted for the analysis of the two satellite datasets is the cross-spectral analysis of longitude-time plots. Figure 6 displays the filtered longitude-time plots of $\log_{10}$(chl) and SSHA, centred at 130°W, 20°S in the South Pacific Ocean, one of the regions with relatively higher cross-correlation (positive peak of 0.55). The cross-spectrum (not shown) has a significant peak at 0.127 deg^{-1} and 2.99 y^{-1}, that is a wavelength of 7.9° and a period of 122 days, with a phase of -0.27 radians, meaning that the signal in $\log_{10}$(chl) lags the signal in SSHA.

Killworth et al. (2003) have applied the cross-spectral technique described above to the global ocean and have found a phase relationship between the two datasets that agrees well, over large parts of the globe, with the phase predicted by a model of horizontal advection of chlorophyll by wave-induced geostrophic velocities. So it would seem that horizontal advection is the prime mechanism responsible for the chlorophyll signal; however, a mismatch in the predicted amplitude of the signal in a number of locations means that a contribution by vertical mechanisms (either vertical advection of phytoplankton, or more likely, vertical advection of nutrients that impact on production) cannot be ruled out at this stage of the research. The definitive answer to the intriguing question on how Rossby waves affect the biology is likely to come from additional comparisons between data and model predictions, in which there is obviously scope for extending the application of cross-spectral techniques to the joint SSHA/SST/chl datasets.

Acknowledgements: The wave-fitting work described in the paper is funded by the EU Satellite-based Ocean ForecasTing (**SOFT**) Project (MAST contr. EVK3-CT-2000-00028).

References

Challenor, P. G., P. Cipollini and D. Cromwell, 2001. Use of the 3-D Radon Transform to examine the properties of oceanic Rossby waves", *J. Atmosph. Ocean. Tech.*, 18, no. 9, 1558-1566 - see also: Corrigendum, *J. Atmosph. Ocean. Tech.*, 19, no. 5, 828, 2002.

Chelton, D. B., and M. G. Schlax, 1996. Global observations of Oceanic Rossby Waves. *Science*, 272, 234-238.

Cipollini, P., D. Cromwell, M. S. Jones, G. D. Quartly, and P. G. Challenor, 1997. Concurrent altimeter and infrared observations of Rossby wave propagation near 34° N in the Northeast Atlantic. *Geophys. Res. Lett*., 24, 889-892.

Cipollini, P., D. Cromwell, P. G. Challenor, and S. Raffaglio, 2001. Rossby waves detected in global ocean colour data. *Geophys. Res. Lett*., 28, 323-326.

Deans, S. R., 1983. *The Radon Transform and Some of Its Applications*, J. Wiley & Sons, 289 pp.

Cromwell, D., 2001. Sea surface height observations of the 34°N 'waveguide' in the North Atlantic *Geophys. Res. Lett.,* 28, 19, 3705-3708.

Gill, A. E., 1982. *Atmosphere-Ocean Dynamics*. Academic Press, 662 pp.

Hill, K. L., I. S. Robinson, P. Cipollini, 2000. Propagation characteristics of extratropical planetary waves observed in the ATSR global sea surface temperature record. *J. Geophys. Res*., 105, 21927-21945.

Killworth, P. D. and J. R. Blundell, 1999. The effect of bottom topography on the speed of long extratropical planetary waves. *J. Phys. Oceanogr*., 29, 2689-2710.

Killworth, P. D. and J. R. Blundell, 2003a: Long extratropical planetary wave propagation in the presence of slowly varying mean flow and bottom topography. Part I: the local problem. *J. Phys. Oceanogr*., 33, 784-801.

Killworth, P. D. and J. R. Blundell, 2003b: Long extratropical planetary wave propagation in the presence of slowly varying mean flow and bottom topography. Part II: ray propagation and comparison with observations. *J. Phys. Oceanogr*., 33, 802-821.

Killworth, P. D., D. B. Chelton, and R. A. de Szoeke, 1997: The speed of observed and theoretical long extratropical planetary waves. *J. Phys. Oceanogr*., 27, 1946-1966.

Killworth, P. D., P. Cipollini, B. M. Uz and J. R. Blundell, 2003: Physical and biological mechanisms for planetary waves observed in sea-surface chlorophyll. *J. Geophys. Res*., submitted.

Quartly, G. D., P. Cipollini, D. Cromwell and P. G. Challenor, 2003. Rossby waves: synergy in action. *Phil. Trans. R. Soc. Lond.*, 361, 57-63.

Siegel, D. A., 2001. The Rossby rototiller. *Nature*, 409, 576-577.

Subrahmanyam, B., I. S. Robinson, J. R. Blundell, and P. G. Challenor, 2001. Indian Ocean Rossby waves observed in TOPEX/POSEIDON altimeter data and in model simulations. *Int. J. Remote Sensing*, 22, 141-167.

Uz, B. M., J. A. Yoder, and V. Osychny, 2001. Pumping of nutrients to ocean surface waters by the action of propagating planetary waves. *Nature*, 409, 597-600.

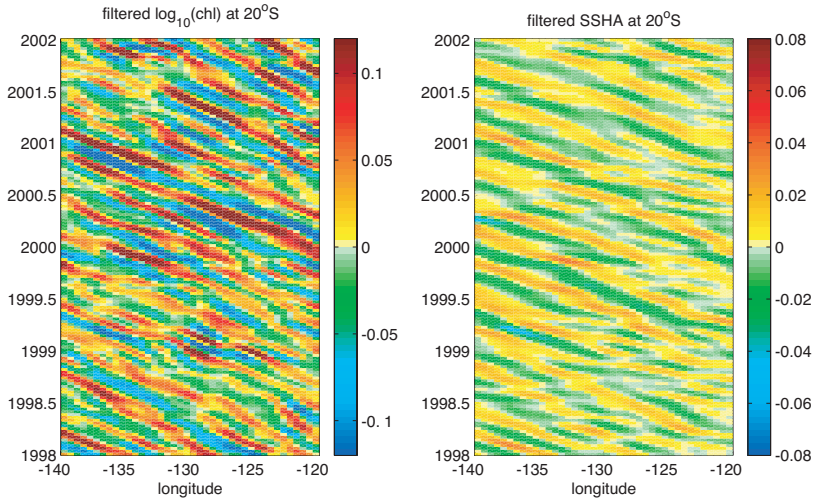

Figure 6: Example of correlation between ocean colour and SSHA. a) filtered longitude/time plot of $\log_{10}$(chl) centred at 130°W, 20°S in the South Pacific Ocean; b) filtered longitude/time plot of SSHA